Received: 31 January 2023 | Revised: 22 March 2023 | Accepted: 7 April 2023

DOI: 10.1002/eom2.12353

EcoMat FUNCTIONAL MATERIALS FOR GREEN ENERGY AND ENVIRONMENT WILEY

RESEARCH ARTICLE

Influence of carbon on the dynamic changes in Co oxidation state of Ba0.5Sr0.5Co0.8Fe0.2O3-δ perovskite catalyst during the oxygen reduction and evolution reactions

Casey E. Beall[1] | **Emiliana Fabbri**[1] | **Adam H. Clark**[2] | **Nur Sena Yüzbasi**[3] | **Thomas Graule**[3] | **Thomas J. Schmidt**[1,4]

[1]Electrochemistry Laboratory, Paul Scherrer Institute (PSI), Villigen PSI, Switzerland

[2]Laboratory for Synchrotron Radiation and Femtochemistry, Paul Scherrer Institute (PSI), Villigen PSI, Switzerland

[3]Laboratory for High Performance Ceramics, Empa, Dübendorf, Switzerland

[4]Laboratory of Physical Chemistry, ETH Zürich, Zürich, Switzerland

Correspondence
Emiliana Fabbri, Paul Scherrer Institute (PSI), 5232 Villigen PSI, Switzerland.
Email: emiliana.fabbri@psi.ch

Funding information
Paul Scherrer Institute; Schweizerischer Nationalfonds zur Förderung der Wissenschaftlichen Forschung, Grant/Award Numbers: Grant PR00P2_193111, Project IZLJZ2_183670

Abstract

Carbon is often used as a conductive additive in catalyst layers to increase conductivity and catalytic activity. However, the effect of carbon addition to perovskites on the oxygen reduction (ORR) and oxygen evolution (OER) reactions is convoluted. In this work, composites of perovskite $Ba_{0.5}Sr_{0.5}Co_{0.8}Fe_{0.2}O_{3-\delta}$ (BSCF) and conductive additives, carbon and indium doped tin oxide are compared. It is found that the conductive additives have differing effects on the ORR and OER activities and cobalt redox behavior, with carbon having a much more significant effect. In order to elucidate further these differences between BSCF and BSCF/carbon, operando X-ray absorption spectroscopy (XAS) is measured simultaneously with cyclic voltammetry into the ORR and OER regions and the continuous changes in the Co oxidation state are observed with high time resolution. We theorize that carbon is enhancing the Co redox activity and as a result, the ORR and OER activities are likewise improved.

KEYWORDS

alkaline, BSCF, cobalt, electrocatalysis, OER, ORR, XAS

1 | INTRODUCTION

With the increased need for energy storage, low temperature alkaline fuel cells and electrolyzers are promising as an energy conversion system. However, the oxygen reduction reaction (ORR) and oxygen evolution reaction (OER) still suffer from high overpotentials and slow kinetics at the cathode and anode sides, respectively. Unified regenerative fuel cells (URFC) are able to switch between fuel cell and electrolyzer mode within the same device, simplifying the amount of components required and therefore the cost. URFCs have been shown to be promising for space, aviation, transportation, and renewable energy applications, particularly when size and mass requirements are restricting. These devices require stable bifunctional oxygen electrodes able to perform both ORR and OER over a large potential range. Perovskites are a low-cost class of materials that have shown activity for

both reactions. Nevertheless, they often suffer from low conductivity. To solve this issue, carbon is often mixed into the catalyst layer, forming a composite electrode (perovskite/carbon), to improve electrical conductivity pathways. The composites have been shown to have varying degrees of OER enhancement, while the improvement to ORR is significantly enhanced.[1–5] The effect of carbon on the ORR activity seems to not be solely based on increased conductivity; the carbon could also be acting as a co-catalyst with the perovskite.[6–11] Oxygen reduction on perovskites is a mixture of 2 and 4-e^- processes, depending on the composition, via a hydrogen peroxide intermediate.[12] Carbon conducts oxygen reduction solely via a 2-e^- pathway to hydrogen peroxide. This hydrogen peroxide can then be further reacted by the perovskite, giving an overall 4-e^- process for perovskite/carbon composites and a higher conversion efficiency.[6–9] Beall et al.[12] gives an in depth discussion of the current synergistic theories.

$Ba_{0.5}Sr_{0.5}Co_{0.8}Fe_{0.2}O_{3-\delta}$ (BSCF)/carbon is a well-studied, promising bifunctional perovskite composite active for both OER and ORR. BSCF without carbon is able to outperform commercial IrO_2 during alkaline membrane water electrolysis testing.[13] However, the ORR activity of BSCF and many other perovskites without carbon is poor and does not match the commercial Pt/C fuel cell performance. Unfortunately, carbon has been shown to degrade at oxidative conditions both during OER and during fuel cell start up and shut down.[14–17] Therefore, a more stable conductive additive needs to be found to replace carbon in the long term for commercialization. In order to find a suitable alternative, it is necessary to understand the exact role of carbon in order to replace it while not losing catalytic activity. One method is to investigate the changes to the catalyst that occur during ORR and OER through operando X-ray absorption spectroscopy (XAS). It was found previously using operando XAS that BSCF forms a Co/Fe oxyhydroxide layer during OER, increasing the average Co oxidation state of the material.[13,18] However, until now, it is unclear how the Co oxidation state of BSCF with and without carbon changes during ORR. Additionally, the continuous changes in Co oxidation state of BSCF have not been investigated during both ORR and OER.

Herein, BSCF is used to investigate the effect of carbon on oxygen electrocatalysis. Two different conductive additives, carbon and indium-doped tin oxide (ITO) nanoparticles, are compared and it is found that carbon leads to much higher catalytic activity as well as redox activity. Then, operando XAS was measured simultaneously with cyclic voltammetry, elucidating continuous changes in the Co oxidation state during the oxygen reduction and evolution reactions. When carbon is added to the catalyst layer, the average Co oxidation state of BSCF is reduced significantly more during oxygen reduction and oxidized moderately more during oxygen evolution. The magnitude of change in oxidation state correlates with catalytic activity and it is theorized why this might be.

2 | RESULTS AND DISCUSSION

To synthesize $Ba_{0.5}Sr_{0.5}Co_{0.8}Fe_{0.2}O_{3-\delta}$ (BSCF), a scalable flame spray method was used in order to produce nanoparticles.[19,20] The synthesized powder has a surface area of about 6.5 ($\pm$ 0.5) m^2/g, determined by BET, and it is composed of a cubic perovskite structure as shown by the XRD pattern and comparison with references (Figure S1) with secondary phases, mostly ascribed to carbonates and nitrates.[19] BSCF was characterized as an oxygen reduction and oxygen evolution reaction catalyst with and without the addition of conductive agents. Acetylene black was chosen due to its common addition to ORR catalyst layers and high conductivity. ITO nanoparticles were chosen as an alternative conductive additive to carbon due to its high conductivity and stability and previous use in electrocatalysis.[21] The conductivity of ITO is slightly less than that of acetylene black. However, the difference between them is insignificant when compared with BSCF, which is many orders of magnitude more resistive (Table S1).

The catalytic activities of BSCF with and without conductive additives were measured using rotating disk electrode (RDE) in oxygen saturated 0.1 M KOH. The ORR and OER activities were measured separately and are shown in Figure 1. The mass normalized Tafel plots are shown in Figure S2. With the addition of carbon, the measured ORR current is increased by more than a factor of 4, while the OER current only by a factor of 1.6. With addition of the conductive additive ITO, the ORR current is increased by a factor of 2 and the OER activity is not affected. When adding a large amount (>25%) of conductive agent of similar conductivity, it is expected to achieve the same catalytic activity. However, they differ significantly on how they affect the two reactions' activities. Therefore, the added conductivity helps to boost oxygen reduction but oxygen evolution is relatively unaffected. Then, additionally, carbon is further positively affecting the ORR and OER activities of BSCF.

When ITO or carbon is added to the catalyst layer, the overall capacitive current increases, as apparent in Figure 1B. Increased capacitive current is an effect of an increased number of electrochemically accessible sites, in this case carbon, ITO, or additional BSCF sites due to increased electrical pathways. Furthermore, the redox

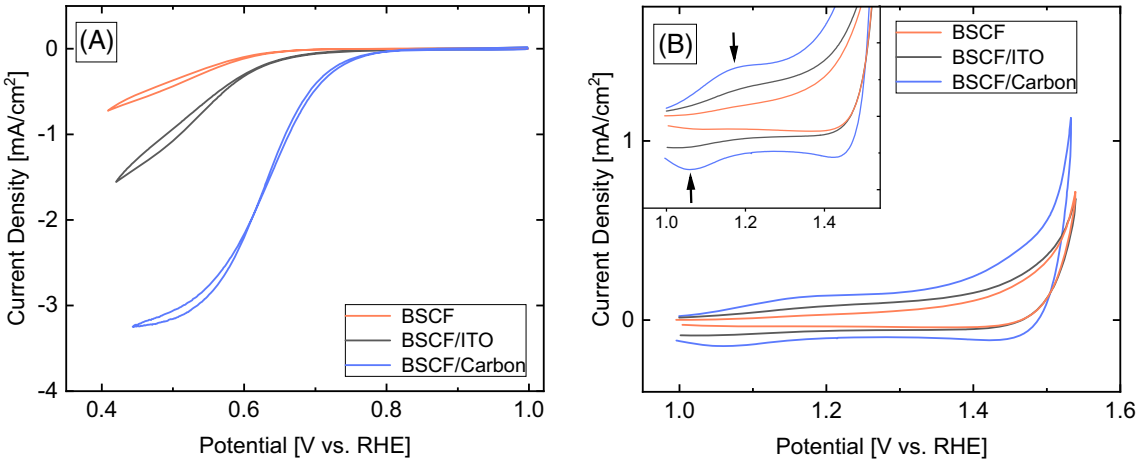

FIGURE 1 Catalytic activity of BSCF determined using RDE in 0.1 M KOH with a rotation rate of 1600 rpm and a scan rate of 5 mV/s with and without different conductive additives for (A) ORR and (B) OER, inset: The change in redox activity with the addition of carbon is highlighted. The arrows highlight the Co(II/III) redox couple at 1.15 V. The ORR current is corrected for capacitance. The catalyst loading (BSCF) was 0.06 mg and the conductive additive (carbon or ITO) was 0.017 mg.

activity is affected by the addition of carbon but not ITO. The $Co^{2+} \leftrightarrow Co^{3+}$ redox transition is present around 1.15 V (Figure 1B). These redox peaks are much more pronounced for the BSCF/carbon composite compared to BSCF/ITO and BSCF as seen in the inset in Figure 1B. With the addition of conductive agents of similar conductivity, it is expected to achieve the same redox activity. However, when comparing these two different conductive additives, carbon provides a larger enhancement of the redox peaks and therefore, the increased redox activity is not solely due to an increased number of electrochemically accessible Co sites. Instead, carbon is seen to be improving the ability of Co to change oxidation state. Overall, it is clear that carbon is enhancing the catalytic activity and redox activity of the perovskite and the reason can only partly be explained by the added conductivity.

To investigate how BSCF changes as a bifunctional catalyst during the oxygen reduction and evolution reactions, an electrochemical protocol was performed where the potential range is widened in a step-wise manner (Figure 2D). Six cyclic voltammetry (CV) cycles were performed in the ORR region (1.0–0.4 V vs. RHE) and with each CV, the upper potential limit was increased up to 1.55 V where oxygen evolution occurs (Figure 2A–C,E–G). With this procedure, the effect of increasingly oxidative potentials on the ORR activity is investigated (Figure 2A–C). For BSCF (Figure 2A), there is no change in the ORR activity during cycles 1–3 (until 1.3 V). After 1.4 V, there is a slight decrease in the oxygen reduction current. Then, after 1.55 V, where OER is actively occurring, there is a significant shift in the ORR onset to higher overpotentials. This is most likely due to the formation of a self-assembled Co/Fe oxyhydroxide layer on the surface of BSCF during OER, as described previously.[13,18,22] This layer most likely blocks the underlying perovskite surface, leading to lower ORR activity for BSCF. The same trend is exactly mirrored for BSCF/ITO (Figure 2B). For BSCF/carbon (Figure 2C), the trend is also mirrored but there is a larger shift in the ORR onset after reaching the upper potentials of 1.4 and 1.55 V. This could possibly be in part due to carbon corrosion, which can occur at high oxidative potentials.

In order to further understand the influence of carbon on the ORR and OER activities and redox behavior, operando XAS was performed at the Co K-edge. The changes in the oxidation state of Co during ORR and OER were measured continuously, simultaneously with the application of the electrochemical protocol, at a rate of one XAS spectra every 5 mV. Cyclic voltammetry was performed with the same protocol as previously, where the potential window is opened into the OER region (Figure 3B). The average Co oxidation states of the pristine materials, both BSCF and BSCF/carbon, are approximately 2.1 suggesting an oxygen defective initial structure, as shown in Figure S3. By measuring XAS continuously during cyclic voltammetry, the continuous Co oxidation state changes are uncovered. Figure 3A clearly shows that these changes depend directly on the applied potential.

There are significant differences in the extent of Co oxidation and reduction that occur when comparing BSCF with and without carbon. Within the first CV into the ORR region (1.0–0.4 V), a clear reduction in the Co oxidation state for BSCF/carbon is observed. Contrarily, no reduction is observed for BSCF alone, instead oxidation is observed. At ORR potentials, the DFT calculated

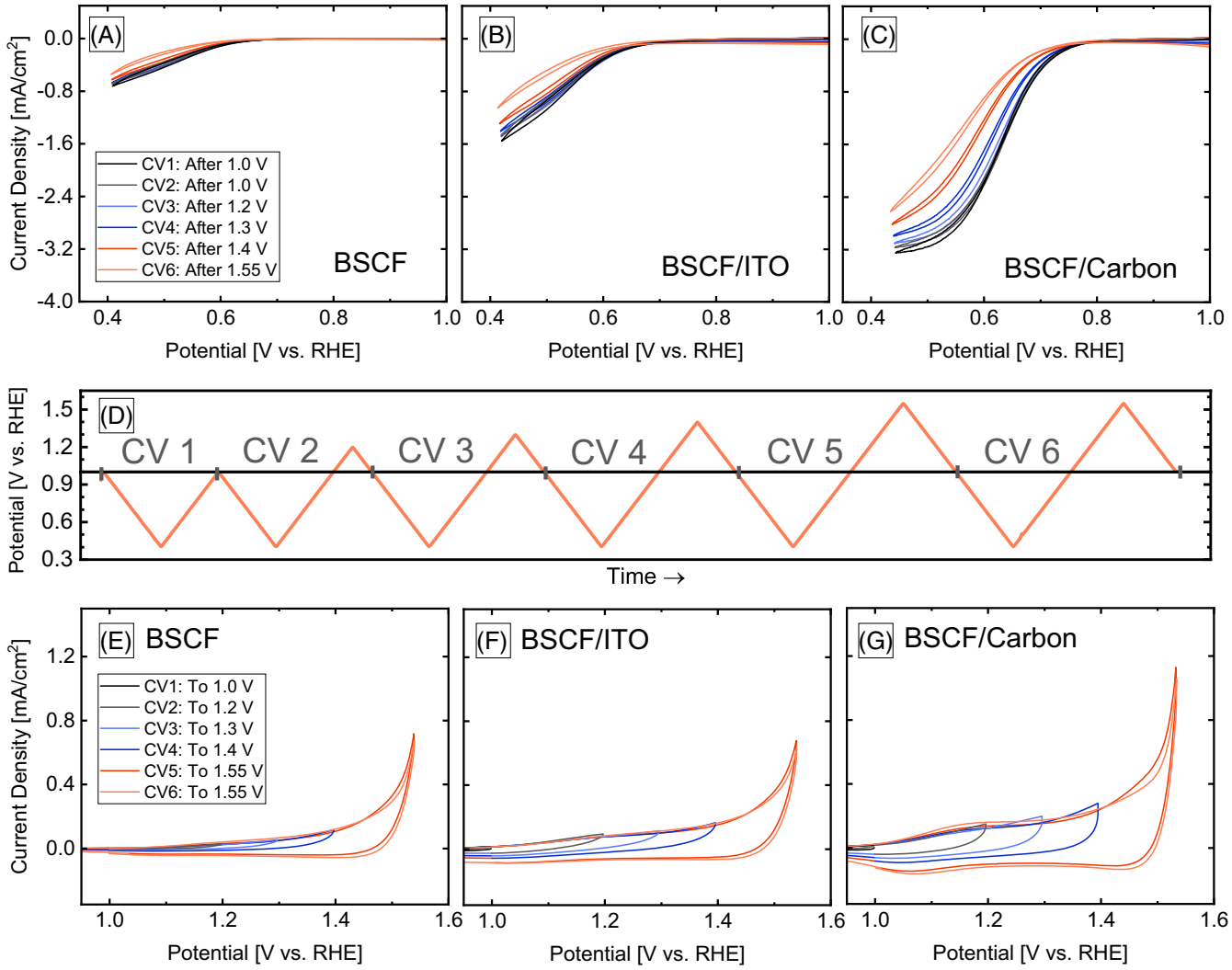

FIGURE 2 ORR and OER activity as the potential window is opened into the oxygen evolution region over 6 CVs using RDE in 0.1 M KOH with a rotation rate of 1600 rpm and a scan rate of 5 mV/s. The (A–C) reductive potentials (0.4–1.0 V) and (E–G) the oxidative potentials (1.0–1.55 V) of the CVs for BSCF, BSCF/ITO, and BSCF/carbon, respectively. (D) The applied potential versus time during 6 cycles of cyclic voltammetry. The catalyst loading (BSCF) was 0.06 mg and the conductive additive (carbon or ITO) was 0.017 mg.

Pourbaix diagram of BSCF predicts the dissolution of Ba and Sr and formation of Co_3O_4 containing $Co^{2.67+}$, significantly more oxidized than Co in BSCF in this study.[18] Therefore, the constant oxidation occurring within the first ORR CV may be due to this electrochemical transformation. Interestingly, the catalyst that is the most reduced during ORR (BSCF/carbon) has the highest ORR activity. It has been shown previously that carbon has a reducing effect on Co in perovskites during the electrode preparation process with ex situ XAS measurements.[1,23] However, in this case the reducing effect occurs during the electrochemical protocol, indicating that ex situ investigations on the role of carbon in perovskite/carbon composites might not be sufficient to fully understand the synergy between perovskite and carbon in the ORR process.

With the second CV, the upper potential is increased to 1.2 V, where the Co(II/III) transition is observed (Figure 1B inset). Consequently, there is a sudden noted jump in the Co oxidation state. This steep increase is much more significant for BSCF/carbon than BSCF and mirrors the differences in the redox peaks seen in Figure 1B. Therefore, the results indicate that the addition of carbon is enhancing the redox capability of Co. During the fourth CV, the onset of OER is reached (around 1.4 V) and both materials suddenly oxidize sharply. Finally, at 1.55 V, where OER is actively occurring, the oxidation states of BSCF and BSCF/carbon become increasingly similar. It is around these potentials where the formation of a self-assembled Co/Fe oxyhydroxide layer occurs on the surface of BSCF.[13,18] With the addition of carbon, the formation of this surface layer is

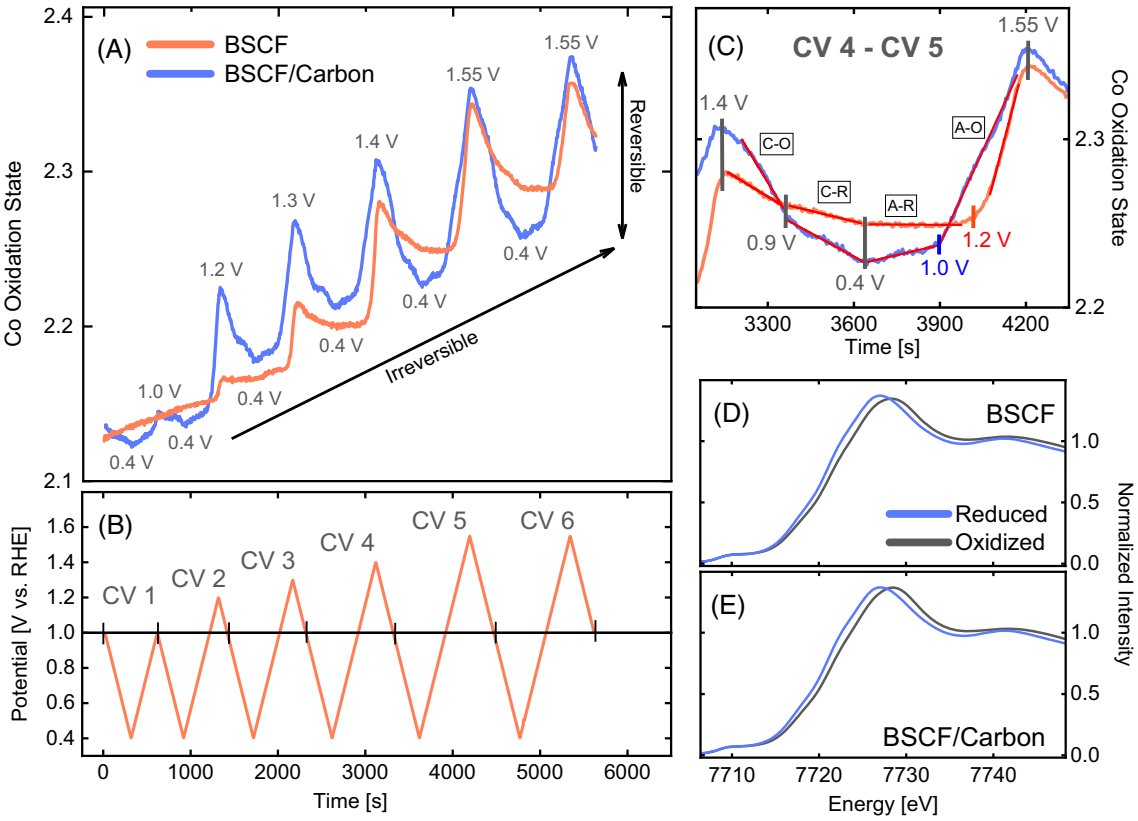

FIGURE 3 (A) Changes in Co oxidation state over time measured by operando XAS as the potential is cycled back and forth between reducing and oxidizing potentials. (B) The applied potential over time during 6 continuous CVs. (C) The region between CVs 4 and 5, which highlights the different linear fit slopes that occur in different potential ranges. The slopes of the labeled regions (cathodic [C], anodic [A], oxidizing [O], and reducing [R]) can be found in Table S2. (D, E) XAS spectra of the most reduced and oxidized states that occur during the 6 CVs.

not hindered, as both experience similar sharp oxidation of Co during OER. Instead, the addition of carbon leads to a higher average Co oxidation state during OER and, subsequently, correlates with a higher OER activity (Figure 1B).

When looking at the trends as a whole in Figure 3A, there are also several characteristic points worth noting. As the potential is cycled between reducing and oxidizing conditions, the Co oxidation state is also reduced and oxidized in a cyclic manner, indicating reversible changes in Co during ORR and OER. For BSCF/carbon, these reversible changes are more significant. Additionally, for both samples there is also an underlying irreversible oxidation occurring with each cycle due to increasing potential and the formation of the oxyhydroxide layer on the surface of BSCF. With each increase in the potential window, the reducing potentials are not able to reverse this oxidation, irrespective of carbon addition.

Due to the high time resolution of the XAS data, the rate of change of Co oxidation state can be estimated at different potentials. The linear fit slopes are shown in Figure 3c and Table S2. During the anodic (A) and cathodic (C) scans, there are four distinct regions with different rates of change of Co oxidation state. The changes in oxidation state under reducing potentials (R) have the slowest kinetics while under oxidizing potentials (O) they are faster. Interestingly, in contrast to each other, the change in oxidation state is faster during the cathodic scan of ORR while for OER, the change in oxidation state during the anodic scan is quicker. Overall, BSCF without carbon has much slower rates of Co oxidation and reduction. The exemption being region A-O, where the rate is faster but oxidation only occurs at higher overpotentials. Therefore, the addition of carbon leads to lower overpotentials for oxidation as well as faster changes in Co oxidation state during ORR and OER.

The catalyst redox capability of Co is shown to play a critical role in promoting increased activity for oxygen electrocatalysis. For both OER and ORR, the magnitude of the change in Co oxidation state trends with the catalytic activities of BSCF and BSCF/carbon. As shown previously, BSCF/carbon experiences an improved redox

capability during ORR than BSCF, suggesting that a more reduced surface is beneficial for ORR. According to the widely accepted ORR mechanism made of four steps and reported as follows, the metal active site changes oxidation state between B^{m+} and $B^{(m-1)+}$ as the reaction proceeds.[12,24–26]

$$B^{(m-1)+} - OH^- + O_2 + e^- \rightarrow B^{m+} - OO^{2-} + OH^- \quad (1)$$

$$B^{m+} - OO^{2-} + H_2O + e^- \rightarrow B^{(m-1)+} - OOH^- + OH^- \quad (2)$$

$$B^{(m-1)+} - OOH^- + e^- \rightarrow B^{m+} - O^{2-} + OH^- \quad (3)$$

$$B^{m+} - O^{2-} + H_2O + e^- \rightarrow B^{(m-1)+} - OH^- + OH^- \quad (4)$$

Oxygen adsorption occurs on the reduced surface (Equation 1) and is where the reaction of HO_2^- (Equation 3) occurs. These steps have been theorized as the rate determining steps.[24,27,28] When carbon is added to the catalyst layer, there is a possible co-catalyst relationship between perovskite and carbon, where the perovskite primarily takes the role of reacting HO_2^-.[6,7,12] Therefore, if a higher percentage of reduced sites are present, the reaction rate is expected to be higher. Additionally, it has been shown that Co in a more reduced state leads to higher ORR activity, when oxygen vacancies are introduced.[29,30] This can be explained by the lifting of the metal d-band center[30] and strengthening of the calculated adsorption energy of oxygen species[31] with reduced Co oxidation state.

During oxygen evolution, the increase of Co oxidation state in BSCF is mostly driven by the formation of an oxyhydroxide layer on the surface, where Co has an oxidation state of about +3. This surface layer is presumably formed on BSCF due to the occurrence of the lattice oxygen evolution reaction (LOER).[32] It is argued that during LOER, the oxygen atoms in the lattice of the perovskite (ABO_3) participate in oxygen evolution, causing A-site dissolution and B-site oxyhydroxide formation.[33] It was shown earlier that the addition of carbon to BSCF leads to a higher Co oxidation state during OER. Therefore, it is possible BSCF/carbon presents a more extended formation of the oxyhydroxide layer due to a higher rate of LOER, which would describe its higher OER activity compared to BSCF.

For both oxygen evolution and reduction, it is clear carbon is greatly affecting the catalytic behavior and Co valence state. One possible theory to explain the role of carbon in the perovskite catalyst layer is that carbon is acting as a redox mediator, facilitating electron transfer during the reduction and oxidation of Co in the perovskite as well as increasing the reaction rate. Various carbon materials have previously been shown to act as redox mediators for applications such as dye degradation and nitroaromatic reduction, speeding up sluggish reaction rates and facilitating dye and nitroaromatic reduction.[34–36] Similarly, in BSCF/carbon composites, the increased redox behavior as well as the faster kinetics of Co oxidation state change in BSCF could be promoted by carbon. It is also possible carbon could be acting as an electron sink for the perovskite electrocatalyst. Although carbon plays an active and convoluted role in ORR, perovskites and perovskite/carbon composites are often not differentiated between or separated in mechanistic studies. Therefore, caution should be taken during mechanistic studies that involve carbon within the catalyst layer, as the valence state of the active cobalt site during ORR and OER is not the same for perovskite and perovskite/carbon composites.

3 | CONCLUSION

Carbon is often added to the catalyst layer of oxygen electrodes to provide conductivity and enhance catalytic activity. However, it is not stable during OER or fuel cell start up and shut down conditions. Therefore, to further commercialization, the role of carbon in the catalyst layer needs to be clarified in order to replace it with another conductive additive. This work investigates $Ba_{0.5}Sr_{0.5}Co_{0.8}Fe_{0.2}O_{3-\delta}$ (BSCF), an active catalyst for both oxygen reduction and evolution, to investigate the addition of carbon as a conductive additive to perovskite catalyst layers. The addition of carbon leads to higher ORR and OER activities compared to another conductive additive, ITO. The improved catalytic performance with the addition of carbon over ITO demonstrates the synergistic effect of carbon on oxygen electrocatalysis above solely a conductivity enhancement. The addition of carbon was found to lead to enhanced Co(II/III) redox capability. To further elucidate these results, operando XAS was measured simultaneously with cyclic voltammetry, where the potential was cycled between reducing and oxidizing regions. BSCF/carbon experienced far larger changes in the Co oxidation state during the protocol, particularly during ORR. We hypothesize that carbon promotes the reduction of Co and as a result, the reduced Co surface is more active for oxygen reduction. Furthermore, carbon addition led to more oxidized Co during OER, which may account for higher LOER rates. By comparing the rate of change of Co oxidation state, we can conclude that the kinetics of Co reduction and oxidation are faster when carbon is added to the catalyst layer.

4 | EXPERIMENTAL SECTION

4.1 | Material synthesis

The perovskite $Ba_{0.5}Sr_{0.5}Co_{0.8}Fe_{0.2}O_{3-\delta}$ was synthesized using the flame spray method described previously.[19,20] The precursor solution consisted of stoichiometric amounts of barium carbonate (≥99.0%, Sigma-Aldrich), strontium nitrate (≥98%, Sigma-Aldrich), cobalt nitrate hexahydrate (99.9%, Sigma-Aldrich), and iron nitrate nonahydrate (≥98%, Sigma-Aldrich) dissolved in Milli-Q water and acetic acid (≥99.0%, Roth) for a total metal concentration of 0.1 M. The flow rate of the precursor was 50 mL min^{-1}, the combustion gas mixture of acetylene (99.6%, Carbagas) and oxygen (99.5%, Carbagas) was 13 L min^{-1} and 17 L min^{-1}, and the dispersion gas (oxygen) was 25 L min^{-1}. Acetylene black (>99.9%, Alfa Aesar) and ITO nanoparticles (25 nm; 99.5%, Fisher Scientific AG) were bought commercially. The Co reference β-CoOOH for XAS was made in house according to the following reference[37] and $Co(OH)_2$ (≥99.9%, Thermo Scientific) was bought commercially.

4.2 | Electrochemical measurements

All electrochemical measurements were performed with a three-electrode set-up using the thin-film rotating disk electrode (RDE) methodology.[38,39] The electrolyte was oxygen saturated 0.1 M KOH (99.99%, Sigma Aldrich). The rotation rate was 1600 rpm and the scan speed was 5 mV s^{-1}. A Hg/HgO reference electrode (RE 61AP, ALS) filled with 0.1 M KOH was used and calibrated against a Pt mesh in hydrogen saturated electrolyte to convert to RHE (0.925 V). All potentials are given versus RHE. A flame annealed gold mesh was the counter electrode. The catalyst ink (15 μL) was dropcasted onto a polished glassy carbon electrode. The ink consisted of BSCF (10 mg), conductive additive (2.8 mg), Milli-Q water (1.5 mL), isopropanol (1 mL), and Na^+-exchanged Nafion (20 μL) (5 wt. %, Sigma Aldrich) as a binding agent and was sonicated for 30 min. All potentials were corrected for ohmic drop using impedance spectroscopy. Currents were normalized by the surface area of the glassy carbon substrate. The ORR activity of the glassy carbon electrode was measured before every dropcast.

4.3 | Material characterization

Powder XRD measurements were made in Bragg–Brentano mode (Smartlab, Rigaku) with Cu Kα radiation. Conductivity was measured using ex situ 4-wire impedance spectroscopy, where the powder samples were compacted into a pellet under 0.6 MPa for 5 min. Then impedance was measured with an amplitude of 500 mV from 1 MHz to 10 mHz. To determine the specific surface area, N_2 adsorption isotherms (Autosorb-1, Quantachrome Instruments) were calculated with Brunauer–Emmett–Teller (BET) analysis. XAS measurements were performed at the SuperXAS beamline at the Swiss Light Source at PSI. The photon beam was produced by a 2.9T superbend magnet, which was collimated with a Si coated mirror at 2.8 mrad and then monochromatized with a channel cut Si (111). Then it was subsequently focused into a size of 0.2 × 1 mm^2 with a double focusing mirror coated with Rh. The ionization chambers contained 1 bar of N_2. The sample was located between the first and second chambers while a Co metal reference foil (99.9%, GoodFellow) was placed between the second and third chambers. All operando measurements were conducted in quick fluorescence mode[40] (using a PIPS detector) while the ex situ Co reference pellets measured in transmission. Data analysis, energy calibration, and normalization were performed with the ProQEXAFS software.[41] Oxidation state calculations are explained in Note S1. The catalyst samples for operando measurements were sprayed (ink consisted of Milli-Q water, isopropanol, and Na^+-exchanged Nafion) onto gold sputtered carbon coated Kapton foil. A homemade flow cell described previously,[42] black pearl (2000 carbon black, Cabot Corporation) sprayed gold sputtered carbon coated Kapton foil counter electrode, and a Ag/AgCl reference electrode (3 M NaCl filled, Harvard Apparatus) were used in a three electrode set-up. The potential of the Ag/AgCl reference electrode was measured versus the Hg/HgO reference electrode described above before every measurement to convert to RHE. Oxygen saturated 0.1 M KOH electrolyte was pulled through the flow cell at a rate of 0.4 mL min^{-1} using a syringe pump.

AUTHOR CONTRIBUTIONS

C.E.B conducted the experimental work and wrote the paper. E.F and T.J.S conceived the project ideas, provided project supervision, results discussion, and financial contribution. A.H.C. assisted in XAS measurements, data analysis, and results discussion. N.S.Y performed the perovskite synthesis. T.J.S. and T.G. provided project supervision and administration. All authors contributed to manuscript revision.

ACKNOWLEDGMENTS

The authors would like to gratefully acknowledge the Swiss National Science Foundation (project IZLJZ2_183670 and

grant No. PR00P2_193111) and the Paul Scherrer Institute for the funding of this work. Furthermore, the authors thank the Swiss Light Source for providing beamtime at the SuperXAS beamline.

CONFLICT OF INTEREST STATEMENT

The authors declare no conflict of interest.

ORCID

Casey E. Beall https://orcid.org/0000-0003-4465-034X

REFERENCES

1. Fabbri E, Nachtegaal M, Cheng X, Schmidt TJ. Superior bifunctional electrocatalytic activity of Ba 0.5 Sr 0.5 Co 0.8 Fe 0.2 O 3-δ /carbon composite electrodes: insight into the local electronic structure. *Adv Energy Mater*. 2015;5(17):1402033. doi:10.1002/aenm.201402033
2. Fabbri E, Mohamed R, Levecque P, Conrad O, Kötz R, Schmidt TJ. Composite electrode boosts the activity of Ba0.5Sr0.5Co0.8Fe0.2O3-δ perovskite and carbon toward oxygen reduction in alkaline media. *ACS Catal.* 2014;4(4):1061-1070. doi:10.1021/cs400903k
3. Mohamed R, Cheng X, Fabbri E, et al. Electrocatalysis of perovskites: the influence of carbon on the oxygen evolution activity. *J Electrochem Soc*. 2015;162(6):F579-F586. doi:10.1149/2.0861506jes
4. Zhu Y, Zhou W, Shao Z. Perovskite/carbon composites: applications in oxygen electrocatalysis. *Small*. 2017;13(12):1603793. doi:10.1002/smll.201603793
5. Nishio K, Molla S, Okugaki T, Nakanishi S, Nitta I, Kotani Y. Effects of carbon on oxygen reduction and evolution reactions of gas-diffusion air electrodes based on perovskite-type oxides. *J Power Sources*. 2015;298:236-240. doi:10.1016/j.jpowsour.2015.08.070
6. Hermann V, Dutriat D, Müller S, Comninellis C. Mechanistic studies of oxygen reduction at La0.6Ca0.4CoO3-activated carbon electrodes in a channel flow cell. *Electrochim Acta*. 2000;46(2–3):365-372. doi:10.1016/S0013-4686(00)00593-4
7. Li X, Qu W, Zhang J, Wang H. Electrocatalytic activities of La0.6Ca0.4CoO3 and La0.6Ca0.4CoO3-carbon composites toward the oxygen reduction reaction in concentrated alkaline electrolytes. *J Electrochem Soc*. 2011;158(5):A597. doi:10.1149/1.3560170
8. Malkhandi S, Trinh P, Manohar AK, et al. Electrocatalytic activity of transition metal oxide-carbon composites for oxygen reduction in alkaline batteries and fuel cells. *J Electrochem Soc*. 2013;160(9):F943-F952. doi:10.1149/2.109308jes
9. Poux T, Bonnefont A, Ryabova A, Kéranguéven G, Tsirlina GA, Savinova ER. Electrocatalysis of hydrogen peroxide reactions on perovskite oxides: experiment versus kinetic modeling. *Phys Chem Chem Phys*. 2014;16(27):13595-13600. doi:10.1039/c4cp00341a
10. Poux T, Bonnefont A, Kéranguéven G, Tsirlina GA, Savinova ER. Electrocatalytic oxygen reduction reaction on perovskite oxides: series versus direct pathway. *ChemPhysChem*. 2014;15(10):2108-2120. doi:10.1002/cphc.201402022
11. Poux T, Napolskiy FS, Dintzer T, et al. Dual role of carbon in the catalytic layers of perovskite/carbon composites for the electrocatalytic oxygen reduction reaction. *Catal Today*. 2012;189(1):83-92. doi:10.1016/j.cattod.2012.04.046
12. Beall CE, Fabbri E, Schmidt TJ. Perovskite oxide based electrodes for the oxygen reduction and evolution reactions: the underlying mechanism. *ACS Catal.* 2021;11(5):3094-3114. doi:10.1021/acscatal.0c04473
13. Fabbri E, Nachtegaal M, Binninger T, et al. Dynamic surface self-reconstruction is the key of highly active perovskite nano-electrocatalysts for water splitting. *Nat Mater*. 2017;16(9):925-931. doi:10.1038/nmat4938
14. Meyers JP, Darling RM. Model of carbon corrosion in PEM fuel cells. *J Electrochem Soc*. 2006;153(8):A1432. doi:10.1149/1.2203811
15. Kinoshita K. *Carbon Electrochemical and Physicochemical Properties*. New York, NY: John Wiley Sons; 1988.
16. Ross PN, Sokol H. The corrosion of carbon black anodes in alkaline electrolyte: I . Acetylene black and the effect of cobalt catalyzation. *J Electrochem Soc*. 1984;131(8):1742-1750. doi:10.1149/1.2115953
17. Filimonenkov IS, Bouillet C, Kéranguéven G, Simonov PA, Tsirlina GA, Savinova ER. Carbon materials as additives to the OER catalysts: RRDE study of carbon corrosion at high anodic potentials. *Electrochim Acta*. 2019;321:134657. doi:10.1016/j.electacta.2019.134657
18. Kim B-J, Fabbri E, Abbott DF, et al. Functional role of Fe-doping in Co-based perovskite oxide catalysts for oxygen evolution reaction. *J Am Chem Soc*. 2019;141(13):5231-5240. doi:10.1021/jacs.8b12101
19. Aegerter D, Borlaf M, Fabbri E, et al. Tuning the Co oxidation state in Ba0.5Sr0.5Co0.8Fe0.2O3-δ by flame spray synthesis towards high oxygen evolution reaction activity. *Catalysts*. 2020;10(9):984. doi:10.3390/catal10090984
20. Heel A, Holtappels P, Hug P, Graule T. Flame spray synthesis of nanoscale La0.6Sr0.4Co 0.2Fe0.8O3-δ and Ba0.5Sr 0.5Co0.8Fe0.2O3-δ as cathode materials for intermediate temperature solid oxide fuel cells. *Fuel Cells*. 2010;10(3):419-432. doi:10.1002/fuce.200900093
21. Zhao S, Wangstrom AE, Liu Y, Rigdon WA, Mustain WE. Stability and activity of Pt/ITO electrocatalyst for oxygen reduction reaction in alkaline media. *Electrochim Acta*. 2015;157:175-182. doi:10.1016/j.electacta.2015.01.030
22. Cheng X, Fabbri E, Yamashita Y, et al. Oxygen evolution reaction on perovskites: a multieffect descriptor study combining experimental and theoretical methods. *ACS Catal*. 2018;8(10):9567-9578. doi:10.1021/acscatal.8b02022
23. Haas O, Holzer F, Müller S, et al. X-ray absorption and diffraction studies of La0.6Ca0.4CoO3 perovskite, a catalyst for bifunctional oxygen electrodes. *Electrochim Acta*. 2002;47(19):3211-3217. doi:10.1016/S0013-4686(02)00241-4
24. Suntivich J, Gasteiger HA, Yabuuchi N, Nakanishi H, Goodenough JB, Shao-Horn Y. Design principles for oxygen-reduction activity on perovskite oxide catalysts for fuel cells and metal-air batteries. *Nat Chem*. 2011;3(7):546-550. doi:10.1038/nchem.1069
25. Mefford JT, Kurilovich AA, Saunders J, et al. Decoupling the roles of carbon and metal oxides on the electrocatalytic reduction of oxygen on La1-xSrxCoO3-δ perovskite composite electrodes. *Phys Chem Chem Phys*. 2019;21(6):3327-3338. doi:10.1039/c8cp06268d
26. Goodenough JB, Cushing BL. Oxide-based ORR catalysts. *Handbook of Fuel Cells*. John Wiley & Sons, Ltd; 2010. doi:10.1002/9780470974001.f205040
27. Spendelow JS, Wieckowski A. Electrocatalysis of oxygen reduction and small alcohol oxidation in alkaline media. *Phys Chem Chem Phys*. 2007;9(21):2654-2675. doi:10.1039/b703315j

28. Hardin WG, Mefford JT, Slanac DA, et al. Tuning the electrocatalytic activity of perovskites through active site variation and support interactions. *Chem Mater*. 2014;26(11):3368-3376. doi:10.1021/cm403785q
29. Ji D, Fan L, Tao L, et al. The Kirkendall effect for engineering oxygen vacancy of hollow Co3O4 nanoparticles toward high-performance portable zinc–air batteries. *Angew Chemie Int ed*. 2019;58(39):13840-13844. doi:10.1002/ANIE.201908736
30. Lee H, Gwon O, Choi K, et al. Enhancing bifunctional electrocatalytic activities via metal d-band center lift induced by oxygen vacancy on the subsurface of perovskites. *ACS Catal.* 2020;10(8):4664-4670. doi:10.1021/acscatal.0c01104
31. Calle-Vallejo F, Inoglu NG, Su H-Y, et al. Number of outer electrons as descriptor for adsorption processes on transition metals and their oxides. *Chem Sci*. 2013;4(3):1245. doi:10.1039/c2sc21601a
32. Binninger T, Mohamed R, Waltar K, et al. Thermodynamic explanation of the universal correlation between oxygen evolution activity and corrosion of oxide catalysts. *Sci Rep*. 2015;5(1):12167. doi:10.1038/srep12167
33. Fabbri E, Schmidt TJ. Oxygen evolution reaction—the enigma in water electrolysis. *ACS Catal.* 2018;8(10):9765-9774. doi:10.1021/acscatal.8b02712
34. van der Zee FP, Bisschops IAE, Lettinga G, Field JA. Activated carbon as an electron acceptor and redox mediator during the anaerobic biotransformation of azo dyes. *Environ Sci Technol*. 2003;37(2):402-408. doi:10.1021/es025885o
35. Pereira RA, Pereira MFR, Alves MM, Pereira L. Carbon based materials as novel redox mediators for dye wastewater biodegradation. *Appl Catal Environ*. 2014;144:713-720. doi:10.1016/J.APCATB.2013.07.009
36. Amezquita-Garcia HJ, Razo-Flores E, Cervantes FJ, Rangel-Mendez JR. Activated carbon fibers as redox mediators for the increased reduction of nitroaromatics. *Carbon N Y*. 2013;55:276-284. doi:10.1016/J.CARBON.2012.12.062
37. Yang J, Liu H, Martens WN, Frost RL. Synthesis and characterization of cobalt hydroxide, cobalt oxyhydroxide, and cobalt oxide Nanodiscs. *J Phys Chem C*. 2010;114(1):111-119. doi:10.1021/jp908548f
38. Schmidt TJ, Gasteiger HA, Stäb GD, Urban PM, Kolb DM, Behm RJ. Characterization of high-surface-area electrocatalysts using a rotating disk electrode configuration. *J Electrochem Soc*. 1998;145(7):2354-2358. doi:10.1149/1.1838642
39. Schmidt TJ, Gasteiger HA. Rotating thin-film method for supported catalysts. In: Vielstich W, Gasteiger HA, Lamm A, eds. *Handbook of Fuel Cells:Fundamentals, Technology and Applications*. Vol 2. John Wiley & Sons; 2003:316-333.
40. Clark AH, Steiger P, Bornmann B, et al. Fluorescence-detected quick-scanning X-ray absorption spectroscopy. *J Synchrotron Radiat*. 2020;27(3):681-688. doi:10.1107/S1600577520002350
41. Clark AH, Imbao J, Frahm R, Nachtegaal M. ProQEXAFS : a highly optimized parallelized rapid processing software for QEXAFS data. *J Synchrotron Radiat*. 2020;27(2):551-557. doi:10.1107/S1600577519017053
42. Binninger T, Fabbri E, Patru A, et al. Electrochemical flow-cell setup for In situ X-ray investigations. *J Electrochem Soc*. 2016;163(10):H906-H912. doi:10.1149/2.0201610jes

SUPPORTING INFORMATION

Additional supporting information can be found online in the Supporting Information section at the end of this article.

How to cite this article: Beall CE, Fabbri E, Clark AH, Yüzbasi NS, Graule T, Schmidt TJ. Influence of carbon on the dynamic changes in Co oxidation state of Ba0.5Sr0.5Co0.8Fe0.2O3-δ perovskite catalyst during the oxygen reduction and evolution reactions. *EcoMat*. 2023;5(7):e12353. doi:10.1002/eom2.12353